Multiresolution Filtering and Segmentation of Multispectral Images

F. Murtagh[a], C. Collet[b], M. Louys[b], and J.L. Starck[c]

[a] School of Computer Science, Queen's University Belfast, Belfast BT7 1NN, Northern Ireland
[b] Université Strasbourg I, LSIIT, Pôle API, Bd S. Brant, 67400 Illkirch, France
[c] Service d'Astrophysique, SAP/SEDI, CEA-Saclay, 91191 Gif-sur-Yvette Cedex, France.

ABSTRACT

We consider multiple resolution methods for filtering and segmenting multispectral astronomical images. For filtering, we use noise modeling, wavelet transform, and the Karhunen-Loève transform. For segmentation, we use a quadtree followed by the fitting of a Markov model. We illustrate these methods on Hubble Space Telescope near infrared NICMOS camera images.

Keywords: multiband image, filtering, wavelet transform, noise model, segmentation, Markov model

1. INTRODUCTION

Resolution-based image preprocessing includes the wavelet transform, and the quadtree. Such transforms yield a decomposition of an image into resolution scale components. The latter can be used subsequently for noise removal, based on a noise model, or for the fitting of a spatial dependency model such as a Markov model. An alternative powerful transform for giving priority to signal in one's observed data is the Karhunen-Loève transform. We will show the powerfulness of these methods, used in an integrated way, for image enhancement, and for image segmentation. The overall goal in filtering and segmentation is the study of faint image features in costly-produced observed signal. From the observed data, physical processes explaining such data can be inferred.

2. WAVELET KARHUNEN-LOÈVE TRANSFORM

The wavelet transform and the Karhunen-Loève transform both provide means of refining the information content of image signals. We will seek the combined advantages of both transforms on multiband image data.

The wavelet transform (see Starck et al.[1]) of an image produces, at each scale j, a set of zero-mean coefficient values $\{w_j\}$. In the à trous method this set has the same number of pixels as the image and thus this wavelet transform is a redundant one. Furthermore, using a wavelet defined as the difference between the scaling functions of two successive scales ($\frac{1}{2}\psi(\frac{x}{2}) = \phi(x) - \phi(\frac{x}{2})$), the original image c_0, with a pixel at position x, y, can be expressed as the sum of all the wavelet scales and the smoothed array c_p

$$c_0(x,y) = c_p(x,y) + \sum_{j=1}^{p} w_j(x,y) \tag{1}$$

To simplify notation, let us take one index running over all pixels,

$$c_0(k) = c_p(k) + \sum_{j=1}^{p} w_j(k) \tag{2}$$

A summary of the à trous wavelet transform algorithm is as follows.

Author contact information: e-mail f.murtagh@qub.ac.uk

1. Initialize i to 0, starting with an image $c_i(k)$. Index k ranges over all pixels.

2. Increment i, and carry out a discrete convolution of the data $c_i(k)$ using a filter h, yielding $c_{i+1}(k)$. The convolution is an interlaced one, where the filter's pixel values have a gap (growing with level, i) between them of 2^{i-1} pixels, giving rise to the name à trous ("with holes"). "Mirroring" is used at the data extremes.

3. From this smoothing we obtain the discrete wavelet transform, $w_i(k) = c_{i-1}(k) - c_i(k)$.

4. If i is less than the number p of resolution levels wanted, return to step 2.

The set $\mathcal{W} = \{w_0, w_1, ..., w_p, c_p\}$, where c_p is a residual, represents the wavelet transform of the data.

The discrete filter h is derived from the scaling function $\phi(x)$. In our calculations, $\phi(x)$ is a B_3 (cubic) spline, which leads (in one dimension) to the filter $h = (\frac{1}{16}, \frac{1}{4}, \frac{3}{8}, \frac{1}{4}, \frac{1}{16})$. Our 2D implementation is based on two 1D sets of (separable) convolutions. The associated wavelet function is of mean zero, of compact support, with a central bump and two negative side-lobes, and is symmetric in both x and y directions.

An additive Gaussian noise model, supposed for the input image, implies an additive Gaussian noise model at each wavelet resolution scale. Noise filtering is then carried out by thresholding at, for example, 3 σ_j at each resolution scale, j.

The Karhunen-Loève transform, also often referred to as eigenvector, Hotelling transform, or principal component analysis allows us to transform discrete signals into a sequence of uncorrelated coefficients. Considering a vector $D = d_1, ..., d_L$ of L signals or images of dimension N (i.e., N pixels per image), we denote $M = \{m_1, ..., m_L\}$ the mean vector of the population (m_i is the mean of the ith signal d_i). The covariance matrix C of D is defined by $C = (D-M)(D-M)^t$, and is of order $L \times L$. Each element $c_{i,i}$ of C is the variance of d_i, and each element $c_{i,j}$ is the covariance between d_i and d_j. The KLT method consists of applying the following transform to all vectors $x_i = \{d_1(i), ..., d_L(i)\}$ ($i = 1..N$):

$$y_i = \Lambda^{-\frac{1}{2}} A(x_i - M) \tag{3}$$

where Λ is the diagonal matrix of eigenvalues of the covariance matrix C, and A is a matrix whose rows are formed from the eigenvectors of C, ordered following decreasing order of eigenvalues.

Because the rows of A are orthonormal vectors, $A^{-1} = A^t$, and any vector x_i can be recovered from its corresponding y_i by:

$$x_i = \Lambda^{\frac{1}{2}} A^t y_i + M \tag{4}$$

The Λ matrix multiplication can be seen as a normalization. Building A from the correlation matrix instead of the covariance matrix leads to another kind of normalization, and the Λ matrix can be suppressed ($y_i = A(x_i - M)$ and $x_i = A^t y_i + M$). Then the norm of y will be equal to the norm of x.

We suppose now that we have L observations of the same view, e.g. at different wavelengths (or at different epochs, etc.), and denote as d_l one observation, $W^{(l)}$ its wavelet transform, and $w_{l,j,k}$ one wavelet coefficient at scale j and at position k. The standard approach would be to use an orthogonal wavelet transform, and to calculate the correlation matrix C from the wavelet coefficients instead of the pixel values:

$$C_{m,n} = \frac{\sum_{j=1}^{J} \sum_{k=1}^{N_j} w_{m,j,k} w_{n,j,k}}{\sqrt{\sum_{j=1}^{J} \sum_{k=1}^{N_j} w_{m,j,k}^2} \sqrt{\sum_{j=1}^{J} \sum_{k=1}^{N_j} w_{n,j,k}^2}} \tag{5}$$

where J is the number of bands, and N_j is the number of coefficients in the band j.

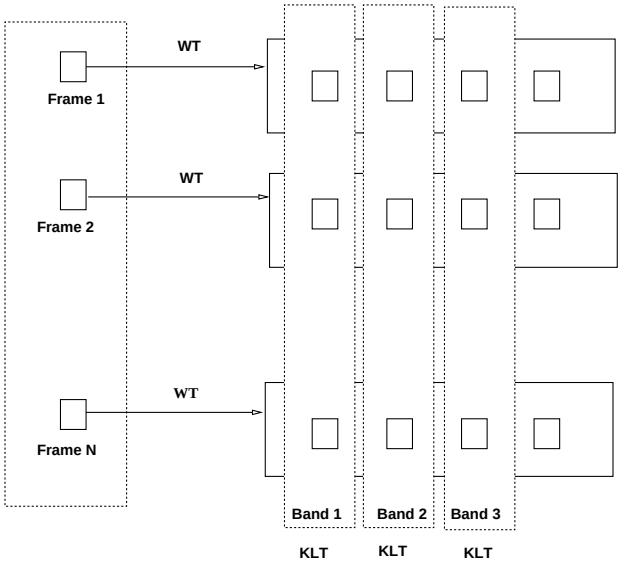

Figure 1. WT-KLT transform flowchart. Each frame of the input data set is first wavelet transformed, and a principal component analysis is applied at each resolution level.

3. HIERARCHICAL MARKOV SEGMENTATION

We now address the problem of segmentation of astronomical multiband images. For segmentation of noisy observed data, Markovian assumptions allow description of global behavior by considering, using a predetermined spatial neighborhood around each pixel, the statistical relation between an observation field and a label field. The latter defines the segmentation. Markov Random Fields (MRFs) lead to iterative, robust procedures which are however slow to converge.[2] To bypass this computational problem, hierarchical modeling allows the definition of different coarse-to-fine strategies, under (spatially and/or in-scale) Markov assumptions.[3] Since the mid-1990s, the hierarchical framework has been extensively studied, with success, for a large variety of applications[4–7] requiring restoration, segmentation or classification steps. In this paper, we consider a special class of Markov models. Causal-in-scale Markov random models, attached to the nodes of a quadtree, are defined in a general manner, allowing us to analyse simultaneously multiband and/or multiresolution images.[8–10] The great interest of this model is that it results in an appealing causality property through scale, which allows the design of exact and non-iterative inference algorithms which are similar to those used in the context of Markov chain models. We present in this paper some results obtained on astronomical multiband images, by using the marginal posterior mode estimator on a quadtree structure: the estimation of the model parameters is then addressed with an expectation-maximization (EM) algorithm, allowing unsupervised hyperparameter estimation. The practical interest of this modeling lies in its generality: the algorithm manages multiresolution and multispectral observed data in a single Causal-in-scale Markov model. It is a useful tool for astronomical images, typically composed of objects of different size, such as stars, galaxies, interstellar clouds, clusters of galaxies, and so on.

Let $G = (S, L)$ be a graph composed of a set S of nodes and a set L of edges. A tree is a connected graph with no cycle where, as a consequence, each node apart from the root r has a unique predecessor, its parent, on the path to the root. A quadtree, as illustrated in Fig. 4, is a tree where each node, apart from the terminal ones or leaves, has four child nodes. The set of nodes S can be partitioned into scales, $S = S^0 \cup S^1 \ldots \cup S^R$, according to the path length of each node to the root. Thus, $S^R = \{r\}$, S^n involves 4^{R-n} sites, and S^0 is the finest scale formed by the leaves. We consider a labeling process X which assigns a class label X_s to each node of G:

$$X = \{X^n\}_{n=0}^{R} \, with X^n = \{X_s, s \in S^n\}\,, \tag{6}$$

where X_s takes its values in the set $\Delta = \{\omega_1, ..., \omega_K\}$, of the K classes. A number of conditional independence

properties are assumed.

First, X is supposed to be Markovian in scale, i.e.,

$$P\left(x^n \left| x^k \right., k > n\right) = P\left(x^n \left| x^{n+1} \right.\right). \tag{7}$$

To simplify notation, we will denote the discrete probability $P(X = x)$ as $P(x)$. It is also assumed that the probabilities of inter-scale transitions can be factorized in the following way:

$$P\left(x^n \left| x^{n+1} \right.\right) = \prod_{s \in S^n} P(x_s \left| x_{s^-} \right.). \tag{8}$$

where s^- designates the single parent of a site s, as illustrated in Fig. 4.

Finally, the likelihood of the observations $\boldsymbol{Y}$ conditional on X is expressed as the following product (assuming conditional independence):

$$P(\boldsymbol{y}|x) = \prod_{n=0}^{R} P(\boldsymbol{y}^n|x^n) = \prod_{n=0}^{R} \prod_{s \in S^n} P(\boldsymbol{y}_s|x_s), \tag{9}$$

where $\forall s \in S^n$, $\forall n \in [0, ..., R]$, and

$$P(\boldsymbol{y}_s|x_s = \omega_i) \stackrel{\triangle}{=} P_i^n(\boldsymbol{y}_s) \tag{10}$$

captures the likelihood of the data y_s, formed by the values in the different channels, at site s of scale n, given label ω_i.

Data are only available at the finest level ($n = 0$) in this paper, but the Markov model on the quadtree is a general model allowing the description of multiresolution observations. Thus, it is appropriate for general multiresolution data segmentation tasks. When no observation exists for $n > 0$, the likelihood $P_i^n(\boldsymbol{y}_s)$ is set to 1. In this way, this approach can be enhanced to handle mixtures of classes.

From these assumptions, it can be easily inferred that the joint distribution $P(x, \boldsymbol{y})$ follows a Gibbs distribution, the expression for which is given by[9]

$$P(x, \boldsymbol{y}) = P(x_r) \prod_{s \neq r} P(x_s|x_{s^-}) \prod_{s \in S} P(\boldsymbol{y}_s|x_s) \tag{11}$$

One of the interests of this model lies in the possibility of computing exactly the posterior marginals $P(X_s|\boldsymbol{Y})$ and $P(X_s, X_s^-|\boldsymbol{Y})$ at each node s within two passes. These computed expressions will be first used in the iterative parameter estimation step.[10] The segmentation label map $\hat{x}$ to be determined is finally given by:

$$\hat{x}_s = \arg\max_{\omega_i \in \Delta} P(X_s = \omega_i | \boldsymbol{Y} = \boldsymbol{y}). \tag{12}$$

This approach provides a powerful tool for processing in an automatic way large quantities of astronomical data.

4. RESULTS OF MULTISPECTRAL ASTRONOMICAL IMAGE ANALYSIS

We applied wavelet-KLT filtering, and segmentation, with success to sets of multispectral images available at Strasbourg Astronomical Observatory. Here we describe use of images of the region M82, from the Hubble Space Telescope Nicmos archive: NIC3 in 6 different wavelengths 1080, 1130, 1640, 1660, 2120, 2150 nm. The WT-KLT processing was carried out on the first five of these bands (with little difference from the processing of all six bands). Fig. 2 displays these six bands.

We considered the following processing path:

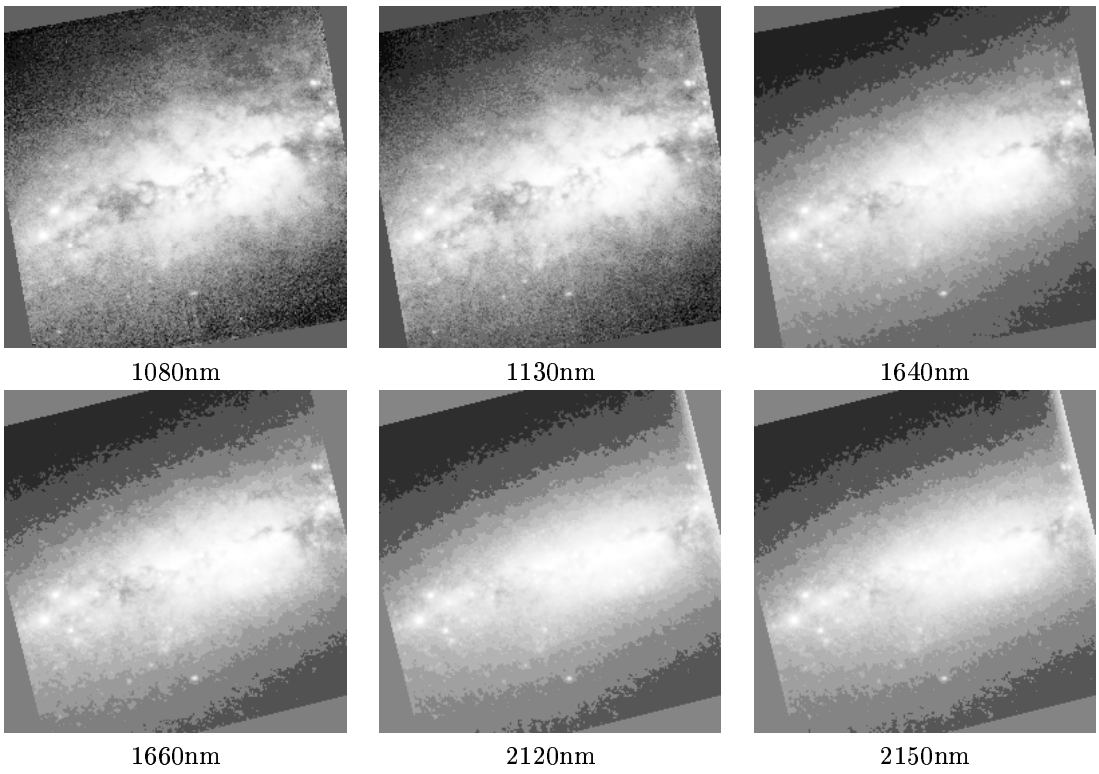

Figure 2. Multiband images of the M82 region, using the Nicmos archive. M82 is the nearest starburst galaxy at a distance of 11 million light years from Earth.

1. Multiresolution image filtering of each band considered separately, using an additive Gaussian noise model, and the B_3 spline à trous wavelet transform. Subsequent processing was carried out on this noise-filtered image set.

2. A KLT was carried out on the five noise-filtered bands, to yield an "eigen-band". Variance explained was found to be 94.2%.

3. We also considered a further WT of the image bands, followed by a KLT at each resolution scale. See Fig. 1. We retained the "eigen-scales", and then applied an inverse WT to them to reconstruct a final image.

Fig. 3 shows the result of 2 above. The outcome of 2 and 3 was found to be very close (mean square error comparison metrics were applied), which both served as mutual confirmation for the result obtained, and also indicated that the additional processing of 3 above could be bypassed.

The segmentation method described in section 3 was applied[11] with success to the same multispectral images. The segmentation result is shown in Fig. 5, resulting from the Markovian-in-scale analysis, taking into account simultaneously the 6 spectral bands.

This approach to segmentation is new and promising. It takes into account a scale decomposition of the information, and the multiband aspects. It provides us with a general fusion model, taking all aspects of the information into account.[12]

Acknowledgments

The authors thank A. Oberto and F. Bonnarel, (CDS, Strasbourg Astronomical Observatory) for software implementation, and A. Lançon for fruitful discussions relating to the M82 images. This research is supported

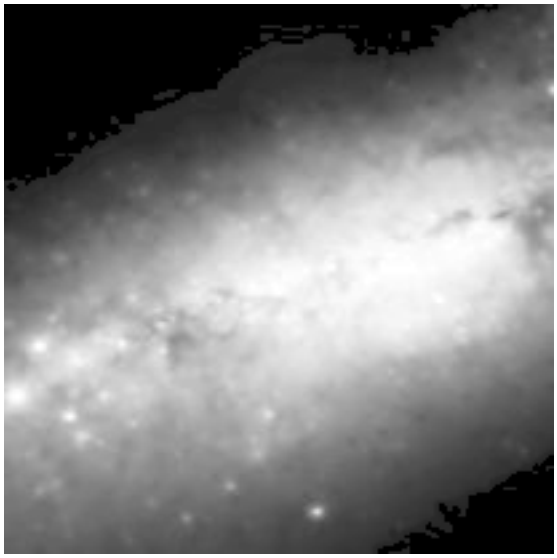

Figure 3. Eigen image band, i.e., principal component of KLT of five image bands, previously noise-filtered using a wavelet transform.

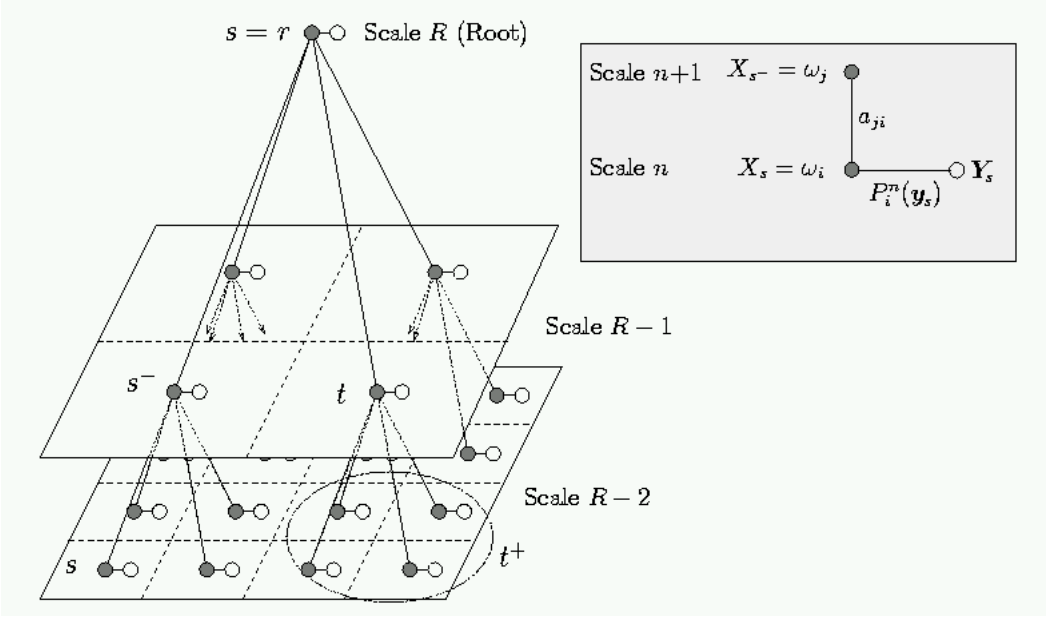

Figure 4. Quadtree structure and its dependency graph. The upper-right gray box shows the Markov link in scale (a_{ij} stands for the probability of down-transition from class ω_j to class ω_i) whereas $P_i^n(\mathbf{y}_s)$ corresponds to the likelihood linking observation $\mathbf{y}_s$ and class label $x_s = \omega_i$

.

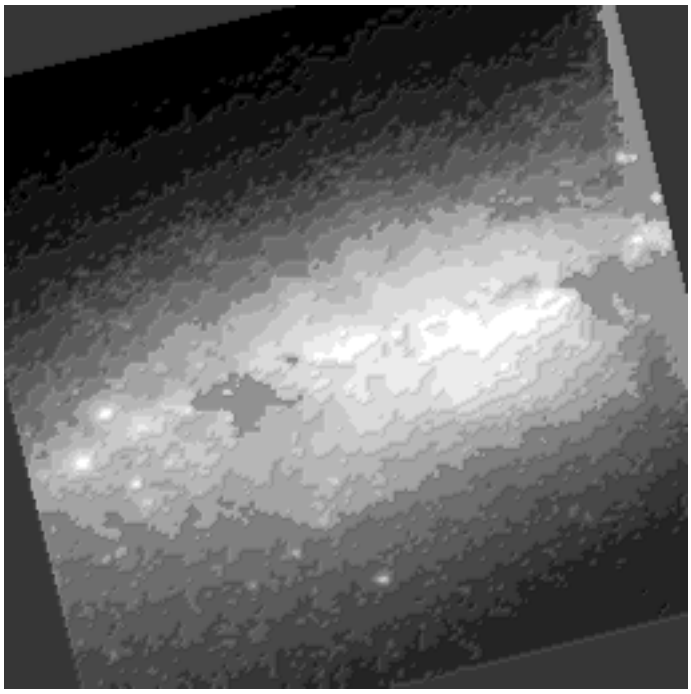

Figure 5. Segmented image using a Markovian-in-scale analysis, taking into account simultaneously the 6 spectral bands. In this single segmentation map, the absorption zones are well detected (dark gray class in the center and middle-right of the image), and the morphology of physical phenomena (geometry, statistical, spectral features) can now be studied in each class separately by using this segmentation map which take into account the entirety of the observations in the 6 bands.

by the French Government ACI-Grid/IDHA project: Action Concertée Incitative-Globalisation des Ressources Informatiques et des Données/Images Distribuées Hétérogènes pour l'Astronomie, 2001-2003.

REFERENCES

1. J. Starck, F. Murtagh, and A. Bijaoui, *Image and Data Analysis: The Multiscale Approach*, Cambridge University Press, 1998.
2. S. Geman and D. Geman, "Stochastic relaxation, Gibbs distributions and the Bayesian restoration of images," *IEEE Trans. Pattern Analysis and Machine Intelligence* **PAMI-6**, pp. 721–741, November 1984.
3. C. Graffigne, F. Heitz, P. Pérez, F. Prêteux, M. Sigelle, and J. Zérubia, "Hierarchical Markov random field models applied to image analysis: a review," in *SPIE Neural Morphological and Stochastic Methods in Image and Signal Processing*, **2568**, pp. 2–17, (San Diego), 10-11 July 1995.
4. P. Pérez and F. Heitz, "Restriction of a Markov Random Field on a graph and multiresolution statistical image modeling," *IEEE Trans. Information Theory* **42:1**, pp. 180–190, 1996.
5. C. Bouman and M. Shapiro, "A multiscale random field model for Bayesian image segmentation," *IEEE Trans. Image Processing* **3**(2), pp. 162–177, 1994.
6. Z. Kato, M. Berthod, and J. Zérubia, "A hierarchical Markov random field model and multitemperature annealing for parallel image classification," *Graphical Models and Image Processing* **58**(1), pp. 18–37, 1996.
7. M. Mignotte, C. Collet, P. Pérez, and P. Bouthemy, "Sonar image segmentation using an unsupervised hierarchical mrf model," *IEEE Trans. Image Processing* **9**, pp. 1–17, July 2000.
8. M. Luettgen, W. Karl, A. Willsky, and R. Tenney, "Multiscale representation of markov random fields," *IEEE Trans. Image Processing* **41**, pp. 3377–3395, December 1993.

9. J.-M. Laferté, P. Pérez, and F. Heitz, "Discrete markov image modeling and inference on the quad-tree," *IEEE Trans. Image Processing* **9**, pp. 390–404, March 2000.
10. P. Rostaing, J.-N. Provost, and C. Collet, "Unsupervised multispectral image segmentation using generalized Gaussian noise model," in *Proc. International Workshop EMMCVPR'99: Energy Minimisation Methods in Computer Vision and Pattern Recognition*, **1654**(Springer-Verlag), pp. 141–156, (York, UK), July 1999.
11. C. Collet, M. Louys, J.-N. Provost, and A. Oberto, "Fusion of astronomical multiband images on a Markovian quadtree," *Information Fusion, http://www.fusion2002.org* , July 2002. Annapolis, Maryland, USA.
12. J. Starck and F. Murtagh, "Astronomical image and signal processing: looking at noise, information and scale," *IEEE Signal Processing Magazine* **18**, pp. 30–40, March 2001.